Probabilistic Estimation of Primary Ship-Induced Wave Heights at Estuary Groins Using a Nonparametric Bayesian Network

Sargol Memar, Ph.D.[1]; Bas Hofland, Ph.D.[2]; Elisa Ragno, Ph.D.[3]; Gregor Melling, Ph.D.[4]; Oswaldo Morales-Nápoles, Ph.D.[5]; Patricia Mares Nasarre, Ph.D.[6]; and Sebastiaan N. Jonkman, Ph.D.[7]

Abstract: Rock groins in the Elbe Estuary are constructed to maintain proper water levels for navigation and for embankment erosion protection. At certain localities, significant damages to rock groins have been observed due to the primary ship-generated waves. Primary waves are generated along the ship's hull and then propagate toward the river banks and groin fields, appearing in the interaction with the structures as a turbulent overflow phenomenon. Eventually, this overflowing may cause damages mainly to the crest and leeward side of the groins. Since this overflowing is the most pronounced with large primary waves at certain water levels, the estimation of the probabilities of extreme primary waves is a key element for a safe and reliable design of groins. For this goal, nonparametric Bayesian networks (NPBNs) are used here to infer the probability distribution function of the extreme primary wave heights at the tip of a groin in the Elbe Estuary. Results demonstrate the suitability of the NPBN in their prediction. The model framework allows the designer to predict the probabilities of primary ship-generated waves at groins when the information of ship dimensions, nautical parameters, and waterway geometry is available. These probabilities can later be used for design purposes for current and future conditions. **DOI: 10.1061/JWPED5.WWENG-2063**.

Introduction

During the last two decades, significant damages to rock infrastructures such as groins have been witnessed along the lower Elbe Estuary, at Juelssand (Germany). The principal reason is the local and temporal alteration of the hydrodynamic regime due to vessel navigation, which is associated with the generation of primary ship-induced wave loads (Melling et al. 2021). The primary ship-generated waves may lead to damages to the river near-bank and bank protections (Fleit et al. 2019). Besides, the development of container fleets has enabled the transit of ever large vessels in the Estuary for the last 25 years (Melling et al. 2021). Ultralarge container vessels in shallow and confined waterways increase the hydrodynamic impact of the ship wave load system along the shoreline (Dempwolff et al. 2022). Hence, for designing rock groins in tidal estuaries, a solution is required to improve their safety and reliability. Accordingly, the estimation of the probabilities of extreme ship-generated primary wave height is a key element. The probabilities of extreme primary wave height can be used for the design of groins given a return period of interest and for reliability analysis and maintenance scheduling.

The prediction and characterization of ship wave loads in rivers and estuaries have been investigated from different perspectives. For instance, Memar et al. (2021) performed a stochastic characterization of ship speed through water, primary wave height, and drawdown at the tip of a groin at Elbe Estuary via extreme value analysis (EVA) and copula modeling. Numerical methods have also been successfully applied to simulate primary ship wave loads (Kochanowski and Kastens 2022; Almström et al. 2021; Bellafiore et al. 2018). In addition to numerical modeling, several empirical equations for the calculation of the ship-generated wave loads have been established for individual ship passages based on field measurements (Ravens and Thomas 2006; Parnell et al. 2016; Huang et al. 2023).

However, these models have practical limitations due to specific regional features of measured data. Moreover, to attain reliable results in a specific study site, more calibration data are required. Generally, empirical and numerical models are deterministic and are based on individual ship passages and typically model cases for which the input values are known and the outcome is observed. In addition, numerical models are time-consuming and computationally expensive. Therefore, these methods do not quantify the

[1]Coastal Engineer, Dept. of Engineering and Estimating, Van Oord Dredging and Marine Contractors, Schaardijk 211, 3063 NH Rotterdam, The Netherlands; Dept. of Hydraulic Engineering, Faculty of Civil Engineering and Geosciences, Delft Univ. of Technology, Delft, The Netherlands (corresponding author). ORCID: https://orcid.org/0000-0003-2980-5067. Email: sargol.memar@vanoord.com

[2]Associate Professor, Dept. of Hydraulic Engineering, Faculty of Civil Engineering and Geosciences, Delft Univ. of Technology, Stevinweg 1, CN 2628 Delft, The Netherlands. Email: b.hofland@tudelft.nl

[3]Assistant Professor, Dept. of Hydraulic Engineering, Faculty of Civil Engineering and Geosciences, Delft Univ. of Technology, Stevinweg 1, CN 2628 Delft, The Netherlands. Email: e.ragno@tudelft.nl

[4]Coastal Engineer, Dept. of Coastal Engineering, Federal Waterways Engineering and Research Institute (BAW), Wedeler Landstr 157, Hamburg 22559, Germany. ORCID: https://orcid.org/0000-0003-2754-0341. Email: gregor.melling@baw.de

[5]Associate Professor, Dept. of Hydraulic Engineering, Faculty of Civil Engineering and Geosciences, Delft Univ. of Technology, Stevinweg 1, CN 2628 Delft, The Netherlands. Email: o.moralesnapoles@tudelft.nl

[6]Lecturer, Dept. of Hydraulic Engineering, Faculty of Civil Engineering and Geosciences, Delft Univ. of Technology, Stevinweg 1, CN 2628 Delft, The Netherlands. Email: p.maresnasarre@tudelft.nl

[7]Professor, Dept. of Hydraulic Engineering, Faculty of Civil Engineering and Geosciences, Delft Univ. of Technology, Stevinweg 1, CN 2628 Delft, The Netherlands. Email: s.n.jonkman@tudelft.nl

Note. This manuscript was submitted on September 11, 2023; approved on December 9, 2024; published online on April 7, 2025. Discussion period open until September 7, 2025; separate discussions must be submitted for individual papers. This paper is part of the ***Journal of Waterway, Port, Coastal, and Ocean Engineering***, © ASCE, ISSN 0733-950X.

probabilities of ship-generated waves; a full range of possible outcomes for the primary waves cannot be calculated. Consequently, existing approaches may lead to under- or overestimation of the primary wave height. To address these issues, this study aims to quantify a multivariate probability distribution function of the ship-generated waves observed at a prototype groin in order to used it for future design assessments.

To achieve this goal, initially, the weekly extreme primary wave heights that may lead to damages to the groin were selected using the EVA method. EVA allows inferring events that have not been observed yet. Afterward, a nonparametric Bayesian network (NPBN) was used to estimate the extreme primary wave height at the tip of the groin when the information of ship dimensions, nautical parameters, waterway geometry, and water level depression along the ship hull is known. The NPBN is used to assign probabilities to different extreme primary wave events. The probabilities of extreme primary wave height can be used for future design conditions and assessment purposes.

NPBNs are graphical tools for statistical inference in which the joint probability distribution of the variables of interest is determined via bivariate pieces of dependence (Hanea et al. 2006), namely, bivariate copulas (Nelsen 2007). In recent years, NPBNs have increasingly been implemented in numerous applications within the civil engineering field due to their numerous advantages. Their computational time is limited, and the uncertainties are embedded in the model. In addition, it allows for the random generation of samples from dependent variables and for making inferences for the variables in the network. Some applications in the civil engineering field are flood risk modeling (Paprotny and Morales-Nápoles 2017), traffic load modeling (Morales-Nápoles and Steenbergen 2015; Mendoza-Lugo et al. 2022), or water resources management (Ragno et al. 2021). Moreover, extensive research can be found in the literature on the use of probabilistic models based on bivariate copulas for seawaves modeling (Antão and Guedes Soares 2014; Jaeger and Morales-Nápoles 2017; Leontaris et al. 2016), highlighting the advantages of these approaches to model their stochastic behavior. Recently, NPBNs have also been proposed to this end in studies to predict the hydrodynamic forces from waves and current loads (Alves et al. 2021) or describe the uncertainty of extreme wind and wave loads (Mares-Nasarre et al. 2023). Alves et al. (2021) concluded that stronger forces were obtained when considering the dependence between the variables, making the use of these models key for structure design. Mares-Nasarre et al. (2023) further assessed the performance of NPBNs to describe the joint probability of extreme wave storms, obtaining a good performance. With all the aforementioned, in this research, we propose the application of NPBNs to model the multivariate uncertainty of extreme primary ship-generated waves.

The paper is organized as follows. First, in the "Physics of Ship-Generated Waves" section, the generation of primary ship-generated wave loads is described. Second, the theoretical framework of Bayesian networks (BNs) is presented in the "Probabilistic Graphical Models: Bayesian Networks" section. Later, the case study groin and data measurements are described in the "Case Study and Data Collection" section. After that, in the "NPBN Model for Ship-Generated Wave Loads" section, the built models, their assessment, the final model, and its application are presented. The results are discussed in the "Discussion" section, and finally, the paper ends with conclusions and remarks.

Physics of Ship-Generated Waves

When a ship travels across a waterway, it displays the water forward, causing a static pressure rise and the creation of a bow wave at the front of the ship. Because of the inertia of motion, the water does not instantly return to equilibrium. This results in fluctuations in the water surface and a swift decline in static pressure along the ship's hull. This appears as a water level depression termed drawdown or Bernoulli wave. The static pressure increases again near the stern of the ship and creates a stern wave behind the ship [Fig. 1(a)] (Sorensen 1997). The pressure changes along the ship's hull are referred to as the primary wave load system, in which the difference between the minimum point of drawdown and maximum point of the stern wave is termed primary wave height H_p (m) and the difference between the minimum point of the drawdown and the ambient water level is termed drawdown Z_a (m) [Fig. 1(a)] (Bhowmik et al. 1981). Primary wave loads impact the banks and bank protections of confined and shallow waterways (Sorensen 1997). The stern wave can appear as an overflowing over the bank protections such as groins, leading to damage to these structures. The characteristics of ship wave loads, such as primary wave height, drawdown, and wave period, depend upon the hydrodynamic field, waterway morphology, and ship properties (Sorensen 1997; Maynord 2005). In shallow and restricted waterways, ultralarge container ships with large immersed cross-sectional areas can induce significant primary ship wave loads. The long-period primary wave load magnitude increases toward the inner waterways as the channel cross section decreases, resulting in a greater blockage and a bigger potential for a large primary wave height. The passing distance from a sailing ship to the river shore or shore protection is another important parameter that influences the magnitude of the primary ship-induced wave load system. The smaller the passing distance, the larger the ship wave loads. To describe the channel blockage, the term blockage factor is used, which is a ratio of the immersed cross-sectional area of the ship and the cross-sectional area of the waterway. However, since the Elbe Estuary is not narrow, to account for the distance of the ship centerline from the groin tip, the partial blockage factor $nT = A_{sp}/A_{cp}$ was introduced by Melling et al. (2021), which is the ratio of the ship's immersed cross section from the ship centerline A_{sp} to the waterway's cross-sectional area from the ship centerline A_{cp} [Fig. 1(b)]. The partial blockage factor is a function of ship draft, ship width, waterway water level, and the distance of the ship centerline and water cross section from the groin tip. By increasing ship speed through water, larger drawdown and primary wave height are generated. However, ships have to adjust their speed to reduce squat and avoid touching the bottom. In shallower water depths, larger ship waves are generated. Considering a certain type of ship passing by a certain channel cross section, when the water depth is low, the partial blockage factor is higher compared to when the water depth is high, resulting in a larger drawdown and primary wave height. However, the largest draft ships travel when the tidal water levels allow them. Large ships have trouble maneuvering at less than approximately 10 knots, since they need sufficient pressure on the rudder. Another factor that has been used to determine the ship-generated wave height is the depth Froude number, which is defined as $U/\sqrt{(gh)}$, where U is the ship speed and h is the water depth of the waterway. For instance, Huang et al. (2023) performed a sensitivity analysis to determine its impact on ship-generated waves. It should be noted that the depth Froude number is based on two of the previously discussed variables: the ship speed and the water depth.

The insights into the physics of ship wave generation, i.e., the influence of each variable on the primary ship-generated waves, and the relationship between variables, described in this section, are used to create the Bayesian Network models, in the "NPBN Model for Ship Wave Loads" section. In the NPBNs, the influence of ship draft, ship width, Estuary water level, and passing distance

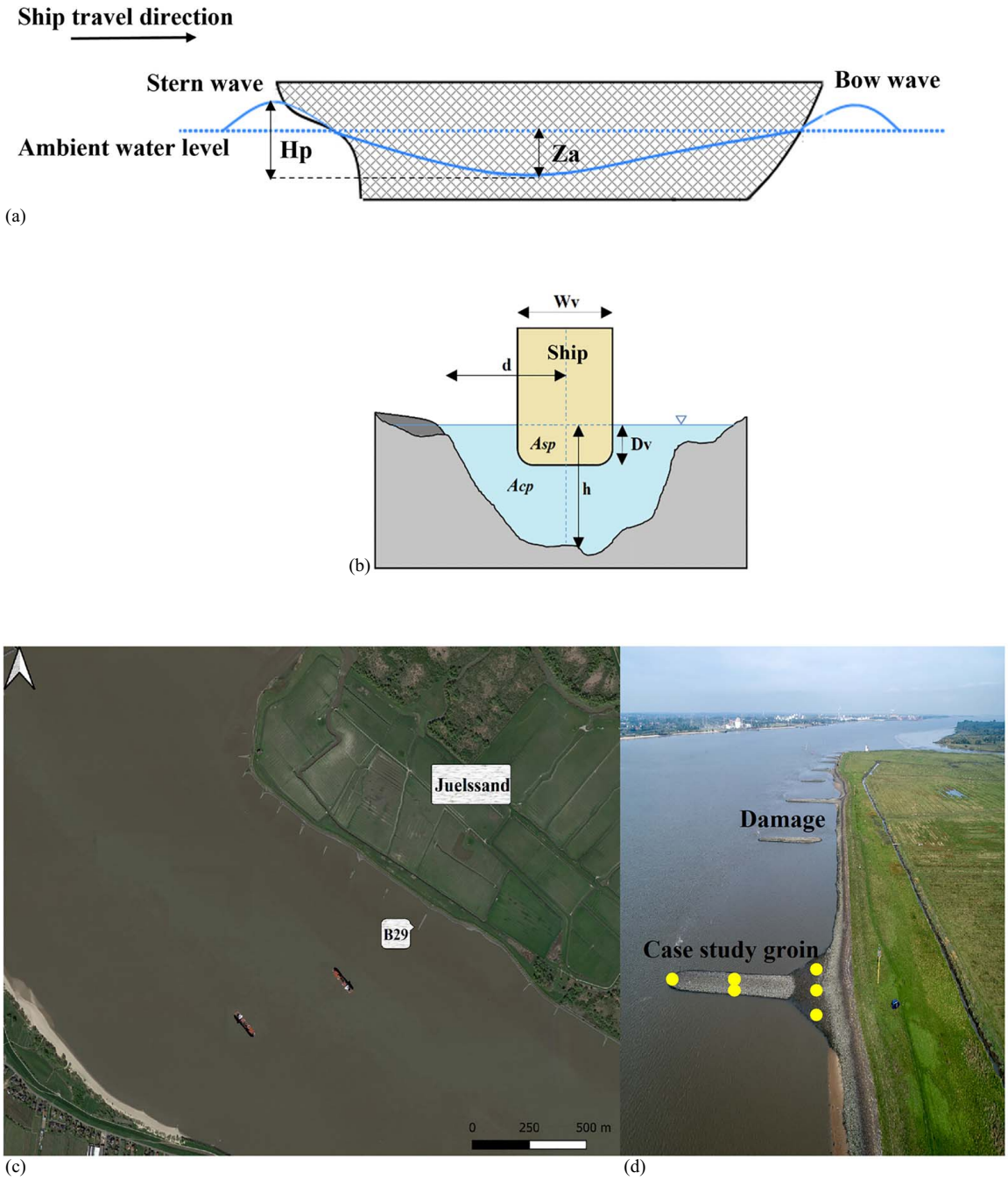

Fig. 1. (a) Primary ship-induced wave loads system; (b) definition of the partial blockage factor (d is the distance of ship from the groin tip, h is the river depth, W_v is the ship width, and D_v is the ship draft); (c) location of the investigated site at Juelssand with the pilot study groin (image data © 2021 Google); and (d) groin field and damage to groins (image courtesy of the Federal Waterways Engineering and Research Institute).

from the ship centerline to the groin tip is addressed using the partial blockage factor variable.

Probabilistic Graphical Models: Bayesian Networks

Bayesian Network

BNs have been identified as an efficient tool for modeling high-dimensional uncertain domains (Aguilera et al. 2011). A BN is composed of a directed acyclic graph (DAG) containing nodes and arcs. The nodes represent random variables, whereas the arcs determine the probabilistic relationship between connected nodes (Neil et al. 2000). The direct predecessors of a node are termed parents, and the direct successors are named children. A graphical representation of BNs enables visualizing the relationships between variables (Hanea et al. 2015). A BN encodes the probability density, or mass function, on a set of random variables $X = \{X_1, \ldots X_n\}$ given a set of conditional independence statements in the DAG coupled with a set of conditional probability functions. It, therefore, enables the representation of a high-dimensional probability distribution function on set X. The conditional independence statements of the network are specified with criteria that are focused on the following possible network pieces

for three random variables $\{X_1, X_2, X_3\}$ (Morales-Nápoles and Steenbergen 2015). Considering Fig. 2, BN1 indicates that X_1 is conditionally independent of X_3 given the information of X_2 ($X_1 \perp X_3 \,|\, X_2$); however, X_1 and X_3 are not marginally independent ($X_1 \perp X_3$). For Bayesian network 2, the criterion is similar to that of Network 1, i.e., stating ($X_1 \perp X_3 \,|\, X_2$); however, ($X_1 \perp X_3$) marginally. Finally, BN3, determines that X_1 is conditionally dependent on X_3 when the information of X_2 is available ($X_1 \perp X_3 \,|\, X_2$) but marginally independent ($X_1 \perp X_3$), which is indicated by the absence of an arc between them. The aforementioned criteria imply that every random variable is independent of its ancestors given its parent. Thus, if every node of the network is associated with a conditional probability density function of that node given its parents $f_{X_i} \,|\, pa(X_i)$, the joint density can be written as follows:

$$f(x_1, x_2, \ldots, x_n) = \prod_{i=1}^{n} f_{X_i \,|\, pa(X_i)}(x_i \,|\, X_{pa(X_i)}) \tag{1}$$

where $pa(X_i)$ = a set of parent nodes X_i. For a node without parents, $pa(X_i) = \varnothing$; thus, $f_{X_i} \,|\, pa(X_i) = f_{X_i}$.

Nonparametric Bayesian Network

The ship wave load model was constructed using an NPBN which is a variant of the BN introduced by Kurowicka and Cooke (2005) and extended by Hanea et al. (2006). In the NPBN, the nodes are specified by invertible marginal distributions and the arcs between the connected nodes are quantified by the (conditional) rank correlation coefficient realized by bivariate normal copula (Kurowicka and Cooke 2005). NPBNs are extensively used for statistical inferences in which the joint probability distribution of the variables of interest is determined via bivariate dependence (Hanea et al. 2015).

The theory of NPBN is centered around bivariate copulas. The bivariate copula or copula of two continuous random variables, X_i and X_j ($i \neq j$), is the function C so that their joint cumulative distribution function is given as $F_{X_i,X_j}(x_i, x_j) = C_\theta(F_{X_i}(x_i), F_{X_j}(x_j))$ (Nelsen 2007; Sklar 1959), where $F_{X_i}(Xi)$ and $F_{X_j}(Xj)$ are the marginal cumulative distribution functions of variables X_i and X_j, respectively. The one-parameter copula C_θ is indexed by the vector of parameter θ, which describes the relationship between the copula and the measures of association between variables, such as Spearman (1904)'s rank correlation (r) or Kendall's tau.

The rank correlation of random variables X_i and X_j is equal to the Pearson product-moment correlation ρ computed with their corresponding cumulative distribution functions F_{Xi} and F_{Xj} as follows:

$$r_{x_i,x_j} = \rho\left(F_{X_i}(x_i), F_{X_j}(x_j)\right) \tag{2}$$

In NPBNs, bivariate normal copulas are implemented to describe the dependence structure between pairs of variables. Hence, the combination of bivariate normal copulas provides the overall dependence structure between all the variables. The normal copula is parameterized by rank correlation; thereby, zero correlations indicate independence. By applying the copula function, the underlying multivariate distribution function is separated from its marginal distributions, which provides high flexibility in presenting the dependence structure of multivariate random variables. Hanea et al. (2006) presented a protocol based on the normal copula assumption to compute the joint distribution function of n random variables $\{X_1, \ldots X_n\}$ having invertible marginal distributions $\{F_1, \ldots F_n\}$.

For each node of a DAG, specified by variable X_i, the variable X_i is transformed into a standard normal variable Y_i with the transformation function $Y_i = \phi^{-1}(F_i(X_i))$, where ϕ^{-1} is the univariate standard normal distribution. The quantity $\rho(X_i, X_j) = 2\sin((\pi/6)r(X_i, X_j))$ is assigned to each arc of the network. Thus, a unique joint normal distribution and a unique correlation matrix R are obtained. Afterward, the R based on partial correlation is computed recursively. Finally, by sampling from the joint normal distribution function of a set of variables Y_i, with correlation matrix R, and then transforming them back to their original units via $\tilde{X}_i = F^{-1}(\phi(\tilde{Y}_i))$, the joint distribution of original variables X_i and their dependence are determined. Additionally, one of the properties of NPBNs is their ability to make probabilistic inferences of a system characteristic (e.g., output) by conditioning on the known characteristics of the system (Kurowicka and Cooke 2002). In this case, the calculated conditioned joint probability distribution function has a smaller dimension compared to the unconditioned network. In this study, to construct the ship wave load model, we used the NPBN based on normal copula assumption implemented in the MATLAB (version 2020) toolbox BANSHEE (Paprotny et al. 2020).

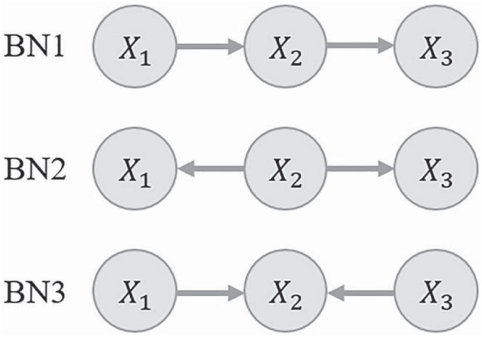

Fig. 2. Illustration of the conditional independence statements of the Bayesian network.

Case Study and Data Collection

The studied groin field is located at Juelssand on the north shoreline of the lower Elbe Estuary, across the main access to the port of Hamburg [Fig. 1(c)]. In this location, considerable damage to the groin field took place due to primary ship-induced wave loads. Therefore, to assess the impact of ship wave loads from different vessel types on the stability of the rock groins, two of the groins were restored using optimized designs based on physical scale model tests and a field study (Melling et al. 2021). The field measurement campaign was carried out with an aim to record a sufficiently long time series of load data on the rebuilt groins. The pressure changes were measured from the mounted pressure sensors (by Driesen and Kern and RBR with a sampling rate of 1 HZ) on the groins at its head, crest, foot, and root areas, which are indicated by gray dots on the groin in Fig. 1(c). The pressure changes are eventually converted to water levels. From the recorded water levels, the primary ship-induced wave loading components, e.g., primary wave height and drawdown, are calculated. The other source of data is the automatic identification system (AIS) data set of vessel traffic. The AIS data set provides high-temporal resolution information about vessel Maritime Mobile Service Identity (MMSI or vessel identification number) and nautical parameters, e.g., ship dimensions (such as ship width and ship length), ship speed through water, ship draft, the passing distance of the ship from the tip of the groin, and ship's position. Over 4,500 ship passages were recorded in the time interval of the field measurements from November 2017 to September 2019.

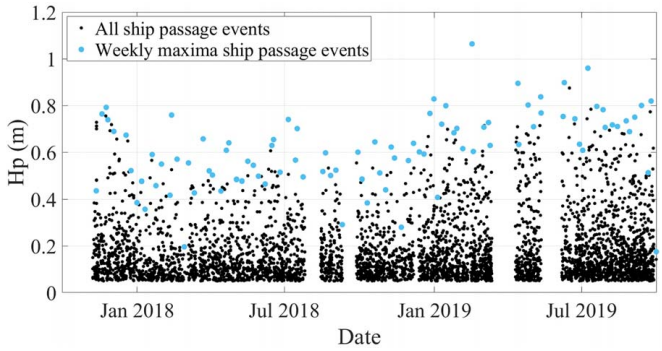

Fig. 3. Time series plot of the measured primary wave height with the specification of the maximum primary wave height within a week.

The extreme primary wave heights can contribute to significant damages to estuarine infrastructures. Therefore, using the extreme value analysis method, maximum values of H_p for each week were selected to create the probabilistic models (93 measurements), while the other variables used in the models are the corresponding events that occur at the same time (concomitant variables) and are not necessarily extreme. As the measured data are available for almost 22 months (from November 2017 to September 2019), weekly maxima data are selected in order to have sufficient measurements to perform a reliable EVA and to create NPBN networks. In Fig. 3, the measurements and the weekly maxima of extreme H_p are depicted. The variables used in the NPBNs are described in more detail in the "NPBN Model for Ship Wave Loads" section. In this study, we used the measurements for the primary wave height and drawdown at the tip of the groin to reduce the influence of groin geometry on the estimated primary waves and ease the extension of the proposed NPBN to other infrastructures in the Elbe Estuary. The maximum recorded primary wave height at the tip of the groin is about 1.06 m. Additionally, this region is characterized by the close ship passing distance (particularly for the seaward passing ships) and significant wave load energy due to small distances between the shoreline and the navigation channel. The distance from the edge of the waterway to the groin tip can be as short as 65 m. The channel side slope is around 1:5. In addition, in this section of the Elbe Estuary, ship speed is restricted (12 knots with a tolerance of 1 knots) and typically vessels travel at their maximum allowed speed.

NPBN Model for Ship Wave Loads

NPBN Orderings and Investigated Networks

The NPBN models are developed based on the AIS and load data sets. A suitable network (DAG) was identified to represent the primary ship-induced wave loads as a system in which (H_p) is given by the interaction between ship and waterway characteristics such as ship speed through water (V_{ship}), ambient water level before ship passage (RWS), partial blockage factor (nT), and ship wave characteristics such as drawdown (Za). Thus, the created NPBN model consists of five continuous random variables: V_{ship}, RWS, nT, Z_a, and H_p (as an output) [Fig. 4(b)]. The characteristics of variables of interest are given in Table 1. The measurements of ambient water levels RWS are 1.5 m above the reference surface geoid.

Network selection to create a dependence model, i.e., expressing the graph representing the physical framework to indicate the relationships between variables involved in the generation of primary ship waves, into a DAG (probabilistic framework) by connecting the nodes with arcs was challenging due to a high number of possible configurations for a DAG describing the set of random variables. Based on our physical understanding of the ship-induced wave generation ("Physics of Ship-Generated Waves" section) and conditional independence statements for NPBN ("Nonparametric Bayesian Networks" section), we tested eight networks (Table 2), all of them with the same nodes but with different parent–child orderings and numbers of arcs [order of variables that determines the (un)conditional correlations in the arcs]. It is identified that the first node of the network can be either V_{ship} or RWS. Thus, two node orderings were investigated: the first node ordering comprises the following variables: V_{ship} (Node 1), RWS (Node 2), nT (Node 3), Z_a (Node 4), and H_p (Node 5) [Fig. 4(a)]. For the second node ordering, the location of Nodes 1 and 2 are substituted thus the ordering is created as RWS, V_{ship}, nT, Z_a, H_p. For each node ordering, four DAGs were constructed based on conditional independence statements for the NPBN and the physical understanding of the ship-generated wave system. For DAG1 and DAG2, the arcs from V_{ship}, RWS, and nT are directly connected to H_p, showing that H_p is unconditionally dependent on ship and waterway characteristics. For DAG3 and DAG4, the arcs from V_{ship}, RWS, and nT are conditionally connected to H_p through Z_a, representing that H_p is conditionally dependent on ship and waterway characteristics. Thus, given the value of Z_a, H_p is independent of the ship and waterway characteristics in this configuration.

The joint probability distribution functions of the variables of the DAGs were then quantified via the associated NPBN. Eventually, the variable of interest, i.e., the primary wave height, can be inferred by conditioning on the remaining variables. The joint distribution function was determined following the procedure presented by Hanea et al. (2006) and is discussed in the previous section. A normal copula was assumed for quantifying (conditional) rank correlations. Furthermore, the marginal distributions of the nodes of the networks were described via both empirical cumulative distribution functions (ECDFs) and parametric probability distribution functions. After performing a sensitivity check for the marginal distributions, the parametric distributions were selected because they allow for generating data beyond the range of observations. In the EVA method, the unseen data are inferred, and this cannot be done by means of ECDF. In Appendix I, the exceedance probability plots of the generated extreme primary wave heights (2,000 samples) using empirical and parametric probability distributions for DAG2 are shown (Fig. 9). The best-fit parametric distribution for every random variable was determined. The following one-dimensional parametric distributions were fitted to the variables: generalized extreme value (GEV), extreme value (EV), normal, Weibull, gamma, inverse Gaussian, logistic, and Rayleigh. The best-fitting probability distributions that described the margins of the NPBN model were selected based on visual inspection and a goodness-of-fit test measure Akaike information criterion (AIC) given as $\text{AIC} = 2K - 2\ln(\hat{L})$, in which K is the number of estimated parameters in the model and $\hat{L}$ is the maximum value of the likelihood function for the model (Akaike 1974). The $2K$ term of AIC is a penalty term for the number of parameters in the likelihood function. The model with the lowest AIC score is expected to be the best model to fit the data while preventing overfitting. The plot of the cumulative distribution functions for the extreme primary wave height for DAG2 is provided (Fig. 10 and Table 5). It was found that the Weibull distribution fitted the best to the extreme primary wave height.

It has to be mentioned that, although in this study the parametric margins were used, the term NPBN is used to be consistent with the previous literature.

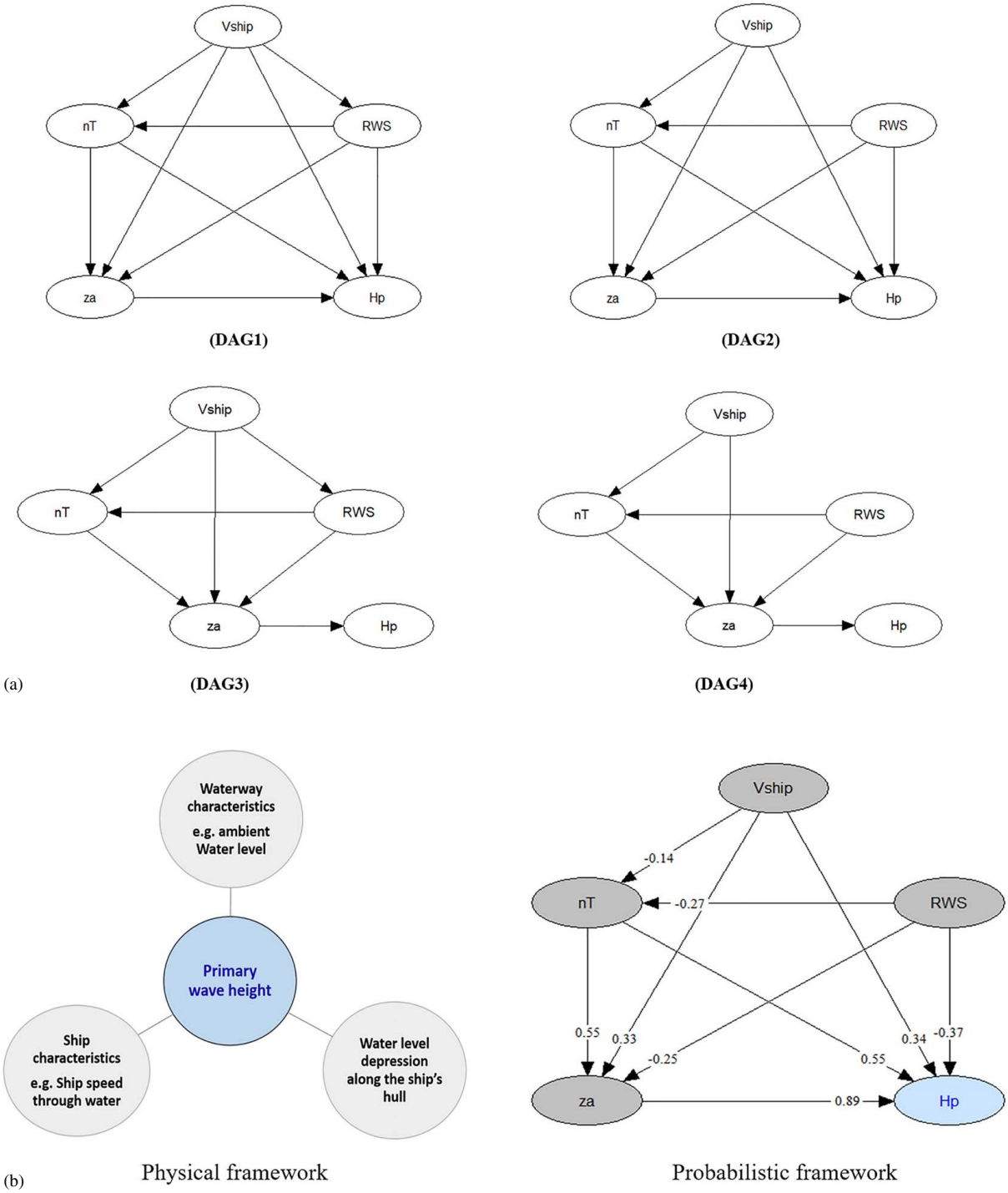

Fig. 4. (a) DAGs of NPBN models for ship-induced wave loads system (sampling order 1); and (b) Physical and probabilistic frameworks for Primary ship-generated wave loads system (probabilistic framework is created in Uninet Software).

Testing the NPBNs

To evaluate the performance of the networks as predictive models, the data were split into 70% and 30% subdata sets for the purpose of training and testing the models, respectively. Predictive modeling uses historical data to create, process, and validate models to identify trends or patterns between data and predict future outcomes. In this study, the diagnostic metrics Nash–Sutcliffe efficiencies (NSE) and Root Mean Square Error (RMSE) were used to evaluate the performance of the models in predicting the primary wave height in both the training and testing subsets.

The NSE is calculated as

$$\mathrm{NSE} = 1 - \frac{\sum_{i=1}^{m} (\mathrm{OBS}_i - \mathrm{SIM}_i)^2}{\sum_{i=1}^{m} (\mathrm{OBS}_i - \overline{\mathrm{OBS}})^2} \tag{3}$$

where SIM and OBS = simulations and observation values, respectively; and $\overline{\mathrm{OBS}}$ mean of observation. Values of NSE > 0.8 indicate a very good model performance (Moriasi et al. 2015), while NSE < 0 suggests that the observations mean is a better predictor compared to the model determined.

Table 1. Characteristics of the variables of interest

Variable	Unit	Description
V_{ship}	knots	Ship speed through water
RWS	mNHN + 1.5 m	Ambient water level (before ship passage)
nT	—	Partial blockage factor
Z_a	m	Difference between ambient and minimum water levels during a primary wave event
H_p	m	Difference between the maximum and minimum water levels during a primary wave event

The RMSE is the standard deviation of the residuals (a measure of how far the data points are from the best-fit line) and is used to compare the prediction errors of different models. In other words, RMSE is a measure of how well a regression line fits the data points. The lower the RMSE, the better a model fits a data set. The formula of RMSE is given according to the following equation:

$$\mathrm{RMSE} = \sqrt{\frac{1}{m}\sum_{i=1}^{m}(\mathrm{SIM}_i - \mathrm{OBS}_i)^2} \tag{4}$$

For both training and testing processes, for every ship passage event, the extreme primary wave height is generated by conditioning on the remaining variables. This is, for each event, the NPBN generates a conditional distribution function of the extreme primary wave height given the variables of V_{ship}, RWS, nT, and Z_a. From the conditional distributions, the medians (50th percentile of a data set) are taken as the simulated H_p for a particular network (DAG). Correspondingly, the 5th and 95th percentiles of the conditional distributions are taken as the confidence intervals of the simulated H_p. Eventually, for all eight DAGs, the observed and simulated (50th) extreme primary wave heights were compared via diagnostic metrics NSE and RMSE (Table 2), calculated on the testing subset. A statistical validation is presented in the Supplemental Material.

Network Selection

The best model among all created networks was selected based on its performance in the estimation of extreme primary wave height using statistical test metrics NSE and RMSE. For this purpose, the observed and simulated (median values of the calculated conditional distribution functions of H_p) extreme primary wave heights were compared via diagnostic metrics. According to Table 2, all networks offer high performances in the estimation of the extreme primary wave height in the testing subset since values of NSE > 0.8 and low values of RMSE < 0.051 (m) are obtained. However, the best model performance is associated with the second network (or DAG2) with the greatest NSE = 0.918 and the smallest RMSE = 0.043 (m) values among other networks. Thus, DAG2 was selected as the best NPBN model for representing the primary ship-generated wave system. In Fig. 4(b), probabilistic framework shows the NPBN model of DAG2 created in the uncertainty analysis software package Uninet (Cooke et al. 2007). The values on the arcs represent the (conditional) rank correlation coefficients between pairs of the network. The variables drawdown and extreme primary wave height are strongly correlated with ship speed through water. Higher ship speeds result in larger water level depressions and consequently larger stern waves. Positive correlations between H_p, Z_a, and nT confirm that when vessels travel toward inner waterways, bigger waves are generated. Ambient water level before ship passage RWS is negatively correlated with nT. This is consistent with reality, since the area of a river cross section at the groin's location becomes smaller in lower water levels, resulting in bigger values of nT. In addition, negative correlations between H_p, Z_a, and RWS demonstrate that in low water levels, the water level depression and primary wave height magnitudes are enlarged along the ship's hull and in the vicinity of shore protection or at the river banks. Eventually, the extreme primary wave heights are associated with the largest drawdowns. The primary wave height is directly connected to the water displacement by the vessel including the return current and the associated water level depression along the hull. Furthermore, the NPBN rank correlation matrix should approximate the empirical rank correlation matrix. These matrices are presented in the Supplemental Material in Tables S1–S4.

Table 2. Results of the test metrics for comparing the observed and predicted extreme primary wave heights (H_p) for different sampling orders and DAGs in the testing subset

DAG	NSE	RMSE	Node ordering
1	0.915	0.044	Vi, RWS, nT, Z_a, H_p
2	0.918	0.043	Vi, RWS, nT, Z_a, H_p
3	0.884	0.051	Vi, RWS, nT, Z_a, H_p
4	0.904	0.047	Vi, RWS, nT, Z_a, H_p
5	0.908	0.0464	RWS, Vi, nT, Z_a, H_p
6	0.912	0.045	RWS, Vi, nT, Z_a, H_p
7	0.886	0.051	RWS, Vi, nT, Z_a, H_p
8	0.87	0.05	RWS, Vi, nT, Z_a, H_p

Validation of the Selected Network

To validate the selected NPBN model (DAG2), five run simulations were performed. Running multiple simulations allows us to validate the accuracy of the models and assess the sensitivity of the results to changes in input parameters. For each simulation run, initially, for every ship passage event, the extreme primary wave height was generated by conditioning on the remaining variables. Afterward, the median (50th percentile of a data set) of the simulated H_p was compared with the observations (Fig. 5). In Fig. 5, the observed weekly maxima primary wave height is compared with the simulated values for the testing model in Runs 1, 2, and 4. It is apparent that most of the observed extreme primary wave heights (for almost 85% of events) fall within the simulated confidence intervals (5th and 95th), which affirms the strength of the model in predicting the extreme primary wave height. The confidence interval between the 5th and 95th is the 90th confidence interval. It is a common practice in coastal engineering (Mares-Nasarre et al. 2023). In fact, the NPBN provides with an estimation of the distribution of H_p, and we typically use the median (50th percentile of a data set) as the estimator. However, the confidence intervals give us more information about the uncertainty. The fact that the observation is within the interval means that the provided distribution by the NPBN is a good approximation; the observation is likely to be a realization of the distribution. Furthermore, Table 3 shows the results of the diagnostic metrics for comparing the simulated and observed extreme primary wave heights for all five run simulations in both training and testing subsets. Values of NSE close to 1 indicate an excellent model performance, while low RMSE values demonstrate the robustness of the model. In addition, resulting values of NSE and RMSE for the training and testing subsets are very close to each other, indicating that the model produces a high level of performance for the unseen data (here testing data). According to these outcomes, the NPBN model demonstrates its suitability in the estimation of extreme primary wave height.

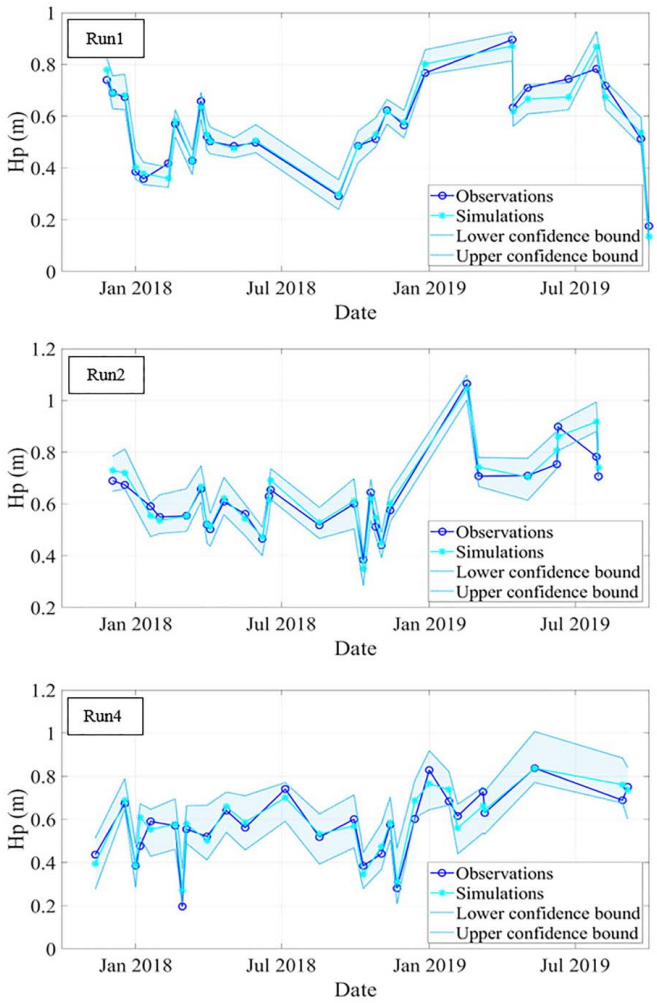

Fig. 5. Comparison between the simulated extreme primary wave heights from Runs 1,2, and 4 and observations for the test data (for DAG2). The shaded area represents the 5th and 95th confidence intervals of the simulated extreme primary wave height.

Besides, the model was further validated by using the NPBN model to infer the primary wave height when the information about variables ambient water level before the ship passage event (RWS) and ship speed through water (V_{ship}) is available (conditional model). To do so, 2,000 samples were generated from the multivariate distribution function of the NPBN. In Fig. 6, the exceedance probability plots of the generated extreme primary wave heights are compared with those of the generated extreme primary wave height when the information about the RWS and V_{ship} is known. For a constant ship speed through water, $V_{ship} = 13$ knots (which is equal to almost 90% of the ship limit speed), two ambient water levels were tested: RWS = 1.77 mNHN + 1.5 m and RWS = 2.37 mNHN + 1.5 m. Considering an arbitrary value of the extreme primary wave height equal to $H_p = 0.8$ m, the probability of the extreme primary wave height exceeding 0.8 m, $p(H_p > 0.8\,\text{m}) = 0.15$ is smaller than the conditional probability of the extreme primary wave height exceeding 0.8 m, given the information V_{ship} and RWS [$p(H_p > 0.8\,\text{m} \mid V_{ship} = 13$ knots and RWS = 1.77 mNHN + 1.5 m) = 0.17]. By increasing the water level, the conditional exceedance probability of the extreme primary wave height is decreased considerably [$p(H_p > 0.8\,\text{m} \mid V_{ship} = 13$ knots and RWS = 2.37 mNHN + 1.5 m) = 0.06]. The results are consistent with reality since the critical situations (the largest primary wave heights) correspond to low water levels and vice versa. Thus, the model proves its applicability in simulating the primary wave height.

Table 3. Test metrics results for comparison between the observed and predicted extreme primary wave heights (H_p) for the training and testing subsets of the DAG2

	Training subset		Testing subset	
Simulation	NSE	RMSE	NSE	RMSE
Run 1	0.918	0.044	0.95	0.029
Run 2	0.917	0.047	0.93	0.037
Run 3	0.908	0.046	0.731	0.09
Run 4	0.941	0.041	0.887	0.048
Run 5	0.928	0.043	0.89	0.048

Example of Model Application

The developed NPBN model can be used to further investigate the influence of variables on the primary wave height. In Fig. 7, the sensitivity of the exceedance probabilities of H_p to RWS and nT is presented. It should be noted that here the variables have been set to three values: one close to the minimum recorded value, one close to the maximum recorded value, and one in between. In this manner, the measured ranges for the different variables are covered and comparison between the plots can be made. As observed in previous research (Bhowmik et al. 1981; Dempwolff et al. 2022), the higher the nT and the lower the RWS, the higher the H_p. This guidance can be used to develop more efficient policies for river management. For instance, it can also be applied to assess the influence of ship speed restrictions for varying water levels. Fig. 8 presents the exceedance probability plot of the extreme primary wave height for different ship speeds when RWS = 1.71(mNHN + 1.5 m). In addition, the

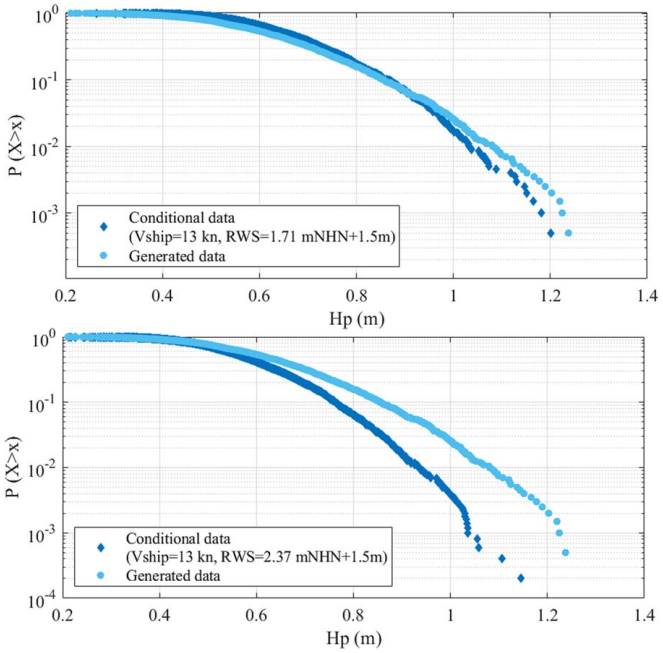

Fig. 6. Exceedance probability plots of generated extreme primary wave heights and generated extreme primary wave heights, given the information about the ship speed (V_{ship}) and ambient water level (RWS) (conditional model) per week.

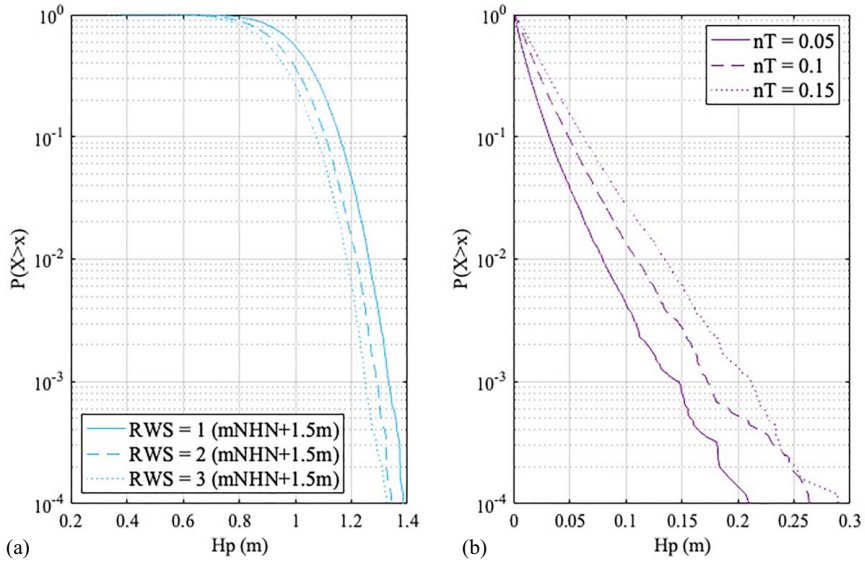

Fig. 7. Sensitivity analysis of the exceedance probabilities of the primary wave height (H_p) to (a) ambient water level (RWS); and (b) partial blockage factor (nT).

probabilities of the extreme primary wave height when the ship speed through water is increased are computed in both low water levels [between 1.2 and 1.71 (mNHN + 1.5 m)] and high water levels [3.2 (mNHN + 1.5 m)], as shown in Table 4). Results indicate that both RWS and V_{ship} have a great influence on the probabilities of exceedance of H_p. In shallower water levels [between 1.2 and 1.71 (mNHN + 1.5 m)], if ships increase their speed from 12.6 to 15 knots, the probabilities of the primary wave height greater than 0.8 m [$P(H_p > 0.8 \mid V_{ship}$, RWS] become almost 3–4.8 times larger. In high water levels [3.2 (mNHN + 1.5 m)], the exceedance probabilities of the primary wave height greater than 0.8 m are increased considerably (36 times). However, these probabilities are smaller than 0.11 (for the highest ship speed 15 knots), showing that shallow waters are more critical for primary wave loading.

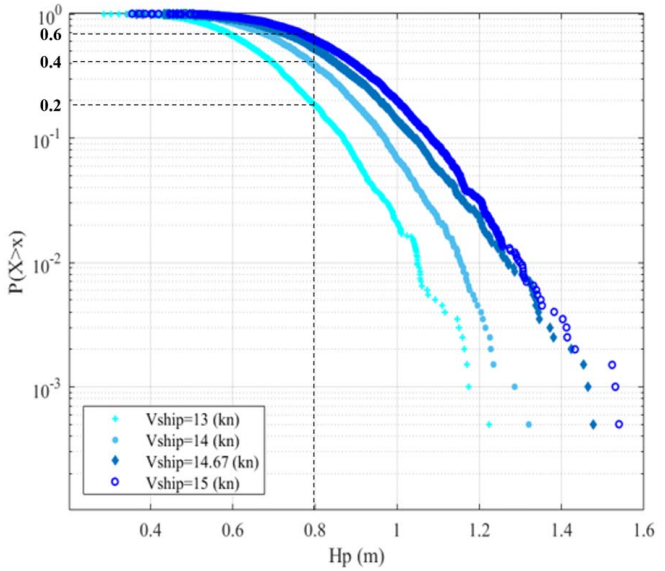

Fig. 8. Exceedance probability plots of the extreme primary wave height for different ship speeds through water when the water level before passage is 1.71 (mNHN + 1.5 m).

Discussion

In this study, the NPBNs were used to estimate the primary wave heights at the tip of a case study groin in the Elbe Estuary. The developed model could be potentially used in the design phase, i.e., to determine proper rock sizes in the groin design through a reliability analysis. A reliability analysis requires the definition of a limit state function, $Z = S - R$, where R is the loading and S is the resistance. Thus, $Z < 0$ implies failure. For groin design, R can be defined as the velocity of the overflow in the leeward side of the groin responsible for the erosion of the rock armor. This velocity can be computed using the primary wave height estimated by the NPBN multiplied by a factor of 2.5. For the considered groin, the measured primary wave height at the crest is an average of almost 2.5 larger than at the tip. Regarding S, it can be defined as the critical flow velocity calculated using Izbash (1936)'s formula which depends on the rock size, between others. Random samples of the primary wave height can be obtained using the NPBN, and they can be propagated through the described methodology to compute the probability of failure of the structure in a Monte Carlo fashion. The obtained probability of failure can be compared to the design one. Further iterations of the process can be performed changing the rock size until the desired probability of failure is obtained. Thus, this model allows to move from a deterministic to a probabilistic design of the studied rock groin and provide further information to the decision-makers about risk levels.

Future research could address the wave–structure interaction directly in the probabilistic model (Mares-Nasarre et al. 2024). That is, variables related to the structure response could be included in the probabilistic model to account for the stochastic nature of such interactions. Within the context of groin design, it would be possible to make a new NPBN that includes variables quantifying the groin damage or further hydrodynamic variables responsible for failure modes, such as the velocities of the groin overflow. However, at the moment, no field measurements are available, and they would need to be calculated through deterministic empirical equations.

It should be noted that the scope of this paper is limited to the case study in the Elbe River, where factors such as the local bathymetry and the groin field have influence on the measured primary

Table 4. Conditional probabilities of extreme primary wave height per week (H_p) for different ship speeds through water and water level before ship passage

V_{ship} (knots)	RWS (mNHN + 1.5 m)	$P(H_p > 0.8 \mid V_{ship}, RWS)$
12.6	1.2	0.24
13	1.2	0.32
13.4	1.2	0.42
14	1.2	0.55
15	1.2	0.76
12.6	1.71	0.12
13	1.71	0.2
13.4	1.71	0.26
14	1.71	0.4
15	1.71	0.6
12.6	3.2	0.003
13	3.2	0.005
13.4	3.2	0.014
14	3.2	0.04
15	3.2	0.11

waves. Therefore, it is encouraged to perform further research on the generalization of this model to different locations and conditions. To do so, databases from field campaigns in locations with different bathymetries, waterway configurations, and traffic compositions would be desired to capture the whole range of possible variations. This would give further insight into the physical processes, especially in the interactions between the waterway bathymetry and the generated primary wave, which has already been highlighted as a key factor in previous studies (Dempwolff et al. 2022). Moreover, it would also be beneficial to perform further field campaigns focused on the structure response to ship-induced loading to better estimate, for instance, the armor damage or the velocity of the groin overflow.

One of the main challenges of using NPBNs is the definition of the DAG. Here, eight possible models are generated based on the physical understanding of the phenomenon and a step-by-step procedure to select and validate it is described. This procedure can be used in future research to define new models in different locations.

Another important assumption of NPBN is the use of Gaussian copulas to model the dependence between the variables. That is, the shape of the dependence between each pair of variables is defined beforehand and the strength of that dependence is given by the rank correlation coefficient. If the dependence does not present significant asymmetries, the Gaussian copula is a reasonable model. Here, asymmetries are observed in some pairs (e.g., tail dependence in the pairs V_{ship} and RWS or RWS and Z_a), although not in most of them. Therefore, these asymmetries were considered negligible, making NPBN an appropriate model. Future research could assess the importance of those asymmetries in other data sets and, if needed, explore the use of models based on copula families different to the Gaussian (Czado 2019).

Conclusions

This study aims to assess the applicability of the NPBN in estimating extreme primary wave heights at the tip of a rock groin situated in the lower Elbe Estuary. The probabilistic framework represents the primary ship-induced wave loads as a system in which the primary wave height is given by the interaction between ship and waterway characteristics and drawdown. Thus, the final network was created using five random variables, namely, ship speed through water, ambient water level before ship passage, partial blockage factor, drawdown, and primary wave height. The NPBN is composed of a directed acyclic graph, which is nonunique, meaning that different networks can be created based on physical understanding of the ship-generated primary wave load system and conditional independence statements of the NPBN. Therefore, eight networks were investigated and a procedure to define, select, and validate them was proposed. Following such procedure, the best network for the estimation of the extreme primary wave height was selected by comparing their performances in generating extreme primary wave height via diagnostic metrics NSEs and RMSE. The good performance of the selected NPBN in terms of NSE and RMSE demonstrates the robustness of the model, highlighting the applicability of NPBNs in general for the estimation of the extreme primary wave height. Also, the proposed model can be used to predict the probabilities of extreme primary wave height on groins in Juelssand for future conditions and for design and assessment purposes.

Appendix I. Empirical vs Parametric Probability Distributions for DAGs

In Figs. 9 and 10, the exceedance probability plots of the generated extreme primary wave heights were compared for both empirical

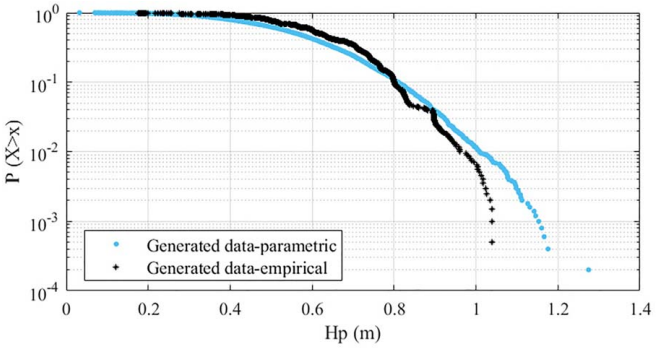

Fig. 9. Comparison between the exceedance probability plots of the generated extreme primary wave heights using empirical cumulative and parametric probability distributions as marginal distributions at the nodes of the NPBN model (DAG2).

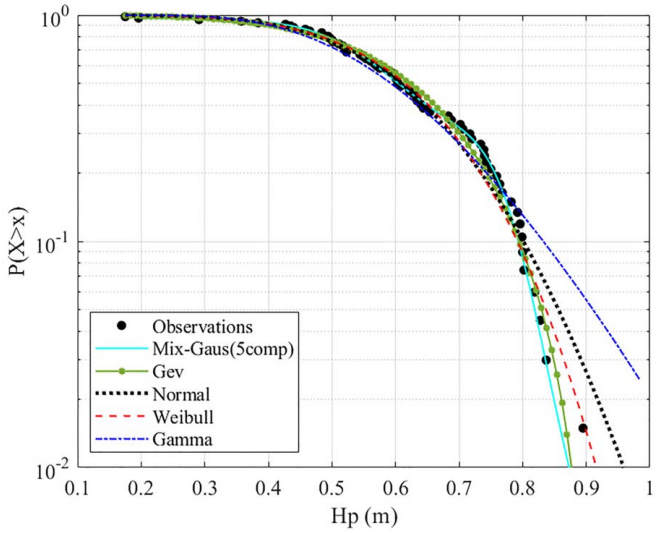

Fig. 10. Fitted distributions to the extreme primary wave heights (for DAG2).

and parametric probability distributions for DAG2. The vertical axis shows the exceedance probabilities $P(X > x) = 1 - P(X \leq x)$ of the extreme primary wave height within a week, while $P(X \leq x)$ is the nonexceedance probability.

Appendix II. AIC-Based Goodness-of-Fit for Extreme Primary Wave Heights

Results of the goodness-of-fit test measure AIC for the determination of the best-fit distribution for the extreme primary wave heights (H_p) are presented in Table 5.

Table 5. Results of the goodness-of-fit test measure AIC for the determination of the best-fit distribution for the extreme primary wave heights (H_p)

Distribution type	Parameters	AIC
GEV	(−0.46, 0.16, 0.56)	−61.28
EV	(0.68, 0.13)	−60.80
Normal	(0.61, 0.15)	−58.34
Weibull	(0.66, 4.75)	−60.43
Gamma	(12.905, 0.05)	−46.65
Inverse Gaussian	(0.61, 6.10)	−34.39
Logistic	(−0.51, 0.15)	−47.52
Rayleigh	(0.44)	−10.11

Data Availability Statement

Some or all data, models, or codes that support the findings of this study are available from the corresponding author upon reasonable request.

Acknowledgments

This research was conducted as part of the ProbBem project, funded by Bundesanstalt für Wasserbau (BAW), and the authors thank the project team for their collaboration and support throughout the research process.

Supplemental Materials

Tables S1–S4 and Figs. S1–S24 are available online in the ASCE Library (www.ascelibrary.org)

References

Aguilera, P. A., A. Fernández, R. Fernández, R. Rumí, and A. Salmerón. 2011. "Bayesian networks in environmental modelling." *Environ. Modell. Software* 26 (12): 1376–1388. https://doi.org/10.1016/j.envsoft.2011.06.004.

Akaike, H. 1974. "A new look at the statistical model identification." *IEEE Trans. Autom. Control* 19 (6): 716–723. https://doi.org/10.1109/TAC.1974.1100705.

Almström, B., D. Roelvink, and M. Larson. 2021. "Predicting ship waves in sheltered waterways—An application of XBeach to the Stockholm Archipelago, Sweden." *Coastal Eng.* 170: 104026. https://doi.org/10.1016/j.coastaleng.2021.104026.

Alves, G. T., O. M. Napoles, and S. N. Jonkman. 2021. "Bayesian networks for estimating hydrodynamic forces on a submerged floating tunnel." In *Proc., 31st European Safety and Reliability Conf.*, 2518–2524. Singapore: Research Publishing Services.

Antão, E., and C. Guedes Soares. 2014. "Approximation of bivariate probability density of individual wave steepness and height with copulas." *Coastal Eng.* 89: 45–52. https://doi.org/10.1016/j.coastaleng.2014.03.009.

Bellafiore, D., L. Zaggia, R. Broglia, C. Ferrarin, F. Barbariol, S. Zaghi, G. Lorenzetti, G. Manfè, F. De Pascalis, and A. Benetazzo. 2018. "Modeling ship-induced waves in shallow water systems: The Venice experiment." *Ocean Eng.* 155: 227–239. https://doi.org/10.1016/j.oceaneng.2018.02.039.

Bhowmik, N. G., M. Demissie, and S. Osakada. 1981. *Waves and drawdown generated by river traffic on the Illinois and Mississippi rivers*. Champaign, IL: Illinois State Water Survey.

Cooke, R., D. Kurowicka, A. Hanea, O. Morales, D. Ababei, B. Ale, and A. Roelen. 2007. "Continuous/discrete non parametric Bayesian belief nets with UNICORN and UNINET." In *Proc., Mathematical Methods in Reliability MMR*, 1–4. Glasgow, UK: s.n.

Czado, C. 2019. *Analyzing dependent data with vine copulas*. Lecture Notes in Statistics 222. Berlin: Springer.

Dempwolff, L.-C., G. Melling, C. Windt, O. Lojek, T. Martin, I. Holzwarth, H. Bihs, and N. Goseberg. 2022. "Loads and effects of ship-generated, drawdown waves in confined waterways—A review of current knowledge and methods." *J. Coastal Hydraul. Struct.* 2: 46–46.

Fleit, G., S. Baranya, T. Krámer, H. Bihs, and J. Józsa. 2019. "A practical framework to assess the hydrodynamic impact of ship waves on river banks." *River Res. Appl.* 35 (9): 1428–1442. https://doi.org/10.1002/rra.v35.9.

Hanea, A., O. M. Napoles, and D. Ababei. 2015. "Non-parametric Bayesian networks: Improving theory and reviewing applications." *Reliab. Eng. Syst. Saf.* 144: 265–284. https://doi.org/10.1016/j.ress.2015.07.027.

Hanea, A. M., D. Kurowicka, and R. M. Cooke. 2006. "Hybrid method for quantifying and analyzing Bayesian belief nets." *Qual. Reliab. Eng. Int.* 22 (6): 709–729. https://doi.org/10.1002/qre.v22:6.

Huang, W., S. Li, Y. Lu, R. Zhang, and H. Wang. 2023. "A new method for predicting the maximum wave height of ship-generated onshore slopes in restricted channel." *Front. Mar. Sci.* 10: 1220975. https://doi.org/10.3389/fmars.2023.1220975.

Izbash, S. 1936. *Construction of dams by depositing rock in running water*. Washington, DC: International Congress on Large Dams.

Jaeger, W. S., and O. Morales-Nápoles. 2017. "A vine-copula model for time series of significant wave heights and mean zero-crossing periods in the North Sea." *ASCE-ASME J. Risk Uncertainty Eng. Syst. Part A: Civ. Eng.* 3 (4): 04017014. https://doi.org/10.1061/AJRUA6.0000917.

Kochanowski, C. A., and M. Kastens. 2022. "Simulation and validation of ship induced waves in shallow and confined water." In *Proc., 6th MASHCON Int. Conf. on Ship Manoeuvring in Shallow and Confined Water, with Special Focus on Port Manoeuvres*, 89–101. Glasgow, UK: Knowledge Centre for Manoeuvring in Shallow and Confined Water.

Kurowicka, D., and R. Cooke. 2005. "Distribution-free continuous Bayesian belief." In *Modern statistical and mathematical methods in reliability*, edited by A. Wilson, S. Keller-McNulty, Y. Armijo, and N. Limnios, 309–322. Singapore: World Scientific.

Kurowicka, D., and R. M. Cooke. 2002. "The vine copula method for representing high dimensional dependent distributions: Application to continuous belief nets." Vol. 1 of *Proc., Winter Simulation Conf.*, 270–278. New York: IEEE.

Leontaris, G., O. Morales-Nápoles, and A. Wolfert. 2016. "Probabilistic scheduling of offshore operations using copula based environmental time series—An application for cable installation management for offshore wind farms." *Ocean Eng.* 125: 328–341. https://doi.org/10.1016/j.oceaneng.2016.08.029.

Mares-Nasarre, P., J. García-Maribona, M. A. Mendoza-Lugo, and O. Morales-Nápoles. 2023. "A copula-based Bayesian network to model wave climate multivariate uncertainty in the Alboran sea." In *Proc., 33rd European Safety and Reliability Conf.*, 1053–1060. Singapore: Research Publishing.

Mares-Nasarre, P., M. R. van Gent, and O. Morales-Nápoles. 2024. "A copula-based model to describe the uncertainty of overtopping variables on mound breakwaters." *Coastal Eng.* 189: 104483. https://doi.org/10.1016/j.coastaleng.2024.104483.

Maynord, S. T. 2005. "Wave height from planning and semi-planning small boats." *River Res. Appl.* 21 (1): 1–17. https://doi.org/10.1002/(ISSN)1535-1467.

Melling, G., H. Jansch, B. Kondziella, K. Uliczka, and B. Gätje. 2021. "Evaluation of optimised groyne designs in response to long-period ship wave loads at Juelssand in the Lower Elbe Estuary." In *Die Küste 89*, 29–56, Karlsruhe: Bundesanstalt für Wasserbau.

Memar, S., O. Morales Napoles, B. Hofland, G. Melling, and G. Melling. 2021. "Characterization of long-period ship wave loading and vessel speed for risk assessment for rock groyne designs via extreme value analysis." In *Proc., 31st European Safety and Reliability Conf.*, 2525–2532. Singapore: Research Publishing Services.

Mendoza-Lugo, M. A., O. Morales-Nápoles, and D. J. Delgado-Hernández. 2022. "A non-parametric Bayesian network for multivariate probabilistic modelling of weigh-in-motion system data." *Transp. Res. Interdiscip. Perspect.* 13: 100552.

Morales-Nápoles, O., and R. D. Steenbergen. 2015. "Large-scale hybrid Bayesian network for traffic load modeling from weigh-in-motion system data." *J. Bridge Eng.* 20 (1): 04014059. https://doi.org/10.1061/(ASCE)BE.1943-5592.0000636.

Moriasi, D. N., M. W. Gitau, N. Pai, and P. Daggupati. 2015. "Hydrologic and water quality models: Performance measures and evaluation criteria." *Trans. ASABE* 58 (6): 1763–1785. https://doi.org/10.13031/issn.2151-0032.

Neil, M., N. Fenton, and L. Nielson. 2000. "Building large-scale Bayesian networks." *Knowl. Eng. Rev.* 15 (3): 257–284. https://doi.org/10.1017/S0269888900003039.

Nelsen, R. B. 2007. *An introduction to copulas*. Berlin: Springer Science & Business Media.

Paprotny, D., and O. Morales-Nápoles. 2017. "Estimating extreme river discharges in Europe through a Bayesian network." *Hydrol. Earth Syst. Sci.* 21 (6): 2615–2636. https://doi.org/10.5194/hess-21-2615-2017.

Paprotny, D., O. Morales-Nápoles, D. T. Worm, and E. Ragno. 2020. "BANSHEE—A MATLAB toolbox for non-parametric Bayesian networks." *SoftwareX* 12: 100588. https://doi.org/10.1016/j.softx.2020.100588.

Parnell, K. E., L. Zaggia, T. Soomere, G. Lorenzetti, and G. M. Scarpa. 2016. "Depression waves generated by large ships in the Venice Lagoon." *J. Coastal Res.* 75 (sp1): 907–911. https://doi.org/10.2112/SI75-182.1.

Ragno, E., M. Hrachowitz, and O. Morales-Nápoles. 2021. "Applying non-parametric Bayesian network to estimate monthly maximum river discharge: Potential and challenges." *Hydrol. Earth Syst. Sci. Discuss.* 2021: 1–25.

Ravens, T., and R. Thomas. 2006. "Ship-wave induced sediment transport in tidal creeks." *WIT Trans. Ecol. Environ.* 88: 121–128.

Sklar, M. 1959. "Fonctions de repartition a n dimensions et leurs marges." *Publ. Inst. Stat. Univ. Paris* 8: 229–231.

Sorensen, R. M. 1997. *Prediction of vessel-generated waves with reference to vessels common to the upper Mississippi river system*. ENV Rep. 4. Vicksburg, MS: US Army Waterways Experiment Station.

Spearman, C. 1904. "The proof and measurement of association between two things." *Am. J. Psychol.* 15 (1): 72–101. https://doi.org/10.2307/1412159.